JOURNAL OF GEOPHYSICAL RESEARCH, VOL. 92, NO. C7, PAGES 6911–6920, JUNE 30, 1987

High-Frequency Internal Wave Observations in the Marginal Ice Zone

STEIN SANDVEN

Nansen Remote Sensing Center, Bergen, Norway

OLA M. JOHANNESSEN

Geophysical Institute, University of Bergen, Bergen, Norway
Nansen Remote Sensing Center, Bergen, Norway

Three thermistor chains extending from 15 to 65 m were deployed from ice floes in the Marginal Ice Zone north of Svalbard in a triangle with sides of 500–800 m for a period of 7 days. Vertical displacement spectra indicate that the internal wave energy level is lower than the Garrett and Munk spectrum by a factor of 2–3 but higher than other observations in the Arctic. A group of internal waves (a wave train), with frequency of 2–3 cph was observed to propagate at 0.05 m/s through the triangle in a west-southwesterly direction during a 4- to 6-hour period. A case study of this wave train, where the horizontal phase differences between the three thermistor chains were analyzed, showed wavelengths of 100–200 m and phase velocities of 0.10–0.15 m/s. Observation of the density field and the velocity field indicated that stratification dominated over vertical shear. Consequently, the dispersion relation was calculated by solving numerically the vertical mode equation for internal waves in a shearless ocean. The estimated wavelengths and phase velocities agree with the dispersion relation for first-mode internal waves. The generating mechanisms may be tidal oscillations associated with a seamount located east of the triangle, or ice keels moving in relation to the water creating lee waves in the pycnocline.

1. INTRODUCTION

Internal wave investigations in ice covered regions of the world oceans are few. Experiments from drifting pack ice in the Arctic Ocean indicate a lower energy level of internal waves (hereafter denoted IW) than in other parts of the ocean [*Morison*, 1986]. During the Norwegian Remote Sensing Experiment (NORSEX) in 1979 [*Johannessen et al.*, 1983] a synthetic aperture radar (SAR) image exhibited IW with wavelengths of 400–1000 m just off the ice edge (Figure 1) at approximately 81°35'N, 7°E. This is in the same area where the 1983 experiment took place. Under calm to moderate wind conditions, IW have also manifested themselves in radar images as convergence lines of ice belts [*Johannessen et al.*, 1985]. However, no in situ IW experiments in the marginal ice zone (MIZ) have so far been reported.

One component of the 1983 Marginal Ice Zone Experiment (MIZEX '83), carried out on the Yermak Plateau north of Svalbard, was a 7-day IW experiment staged from R/V *Polarbjørn*, which was moored to a drifting ice floe 20 km in from the ice edge. Three thermistor chains were suspended in a triangle from drifting ice floes. A number of other experiments were run in parallel, describing the ocean, the ice, and the atmosphere [*MIZEX Group*, 1986]. For high-frequency IW studies, the most important data sources were the thermistor chains with sampling frequency well above the Brunt-Väisälä frequency, whereas useful background information came from conductivity-temperature-depth (CTD) casts, Aanderaa current meters, profiling current meters, ice drift, and wind measurements.

In the first part of this paper the experiment and selected IW observations are described. Then energy spectra, horizontal coherence, and phase spectra are estimated, and finally, the dispersion relation is computed and compared with observations.

Paper number 7C0116.
0148-0227/87/006C-0116$05.00

2. DESCRIPTION OF THE EXPERIMENT

Three thermistor chains, designated T46, T47, and T518, were deployed from ice floes in a triangle with sides 500 m, 700 m, and 800 m long. The ice concentration in the area was approximately 90%, and the dominant ice floe dimension was typically 25–100 m (Figure 2). Approximately 10 km farther north, large ice floes (1–20 km) representing the major Arctic pack ice were found. T46 was deployed next to the ship, while T47 and T518 (deployed 500 m and 800 m from the ship, respectively), were positioned relative to the ship using acoustic sensors with an accuracy of a few meters. These position data and the ship's heading showed that the triangle did not change its shape and orientation significantly in the deployment period from June 30 to July 7. To first order, the triangle drifted as a solid body without rotation, although its trajectory is characterized as tidal rotation superimposed on a northeastward linear movement (Figure 3).

Each Aanderaa thermistor chain had temperature sensors at 5-m depth intervals between 15 m and 65 m. The response time of the sensors was approximately 1 min. In order to have independent measurements, a sampling interval of 2 min was used. T518 had a pressure sensor at 65 m which showed that no significant horizontal excursions of the thermistor chain had occurred during the experiment. A current meter mooring was also deployed from an ice floe near the ship, with Aanderaa current meters at 2 m, 10 m, 20 m, 40 m, and 200 m. Throughout the drift period the ship was moored to an ice floe, and the ship's drift was the same as the drift of the thermistor chains: 0.10–0.20 m/s. Wind data from the ship showed wind speeds to be calm to moderate, 2–5 m/s, throughout the experiment. During the first 4–5 days the wind direction was from the south-southwest, but on July 4 it

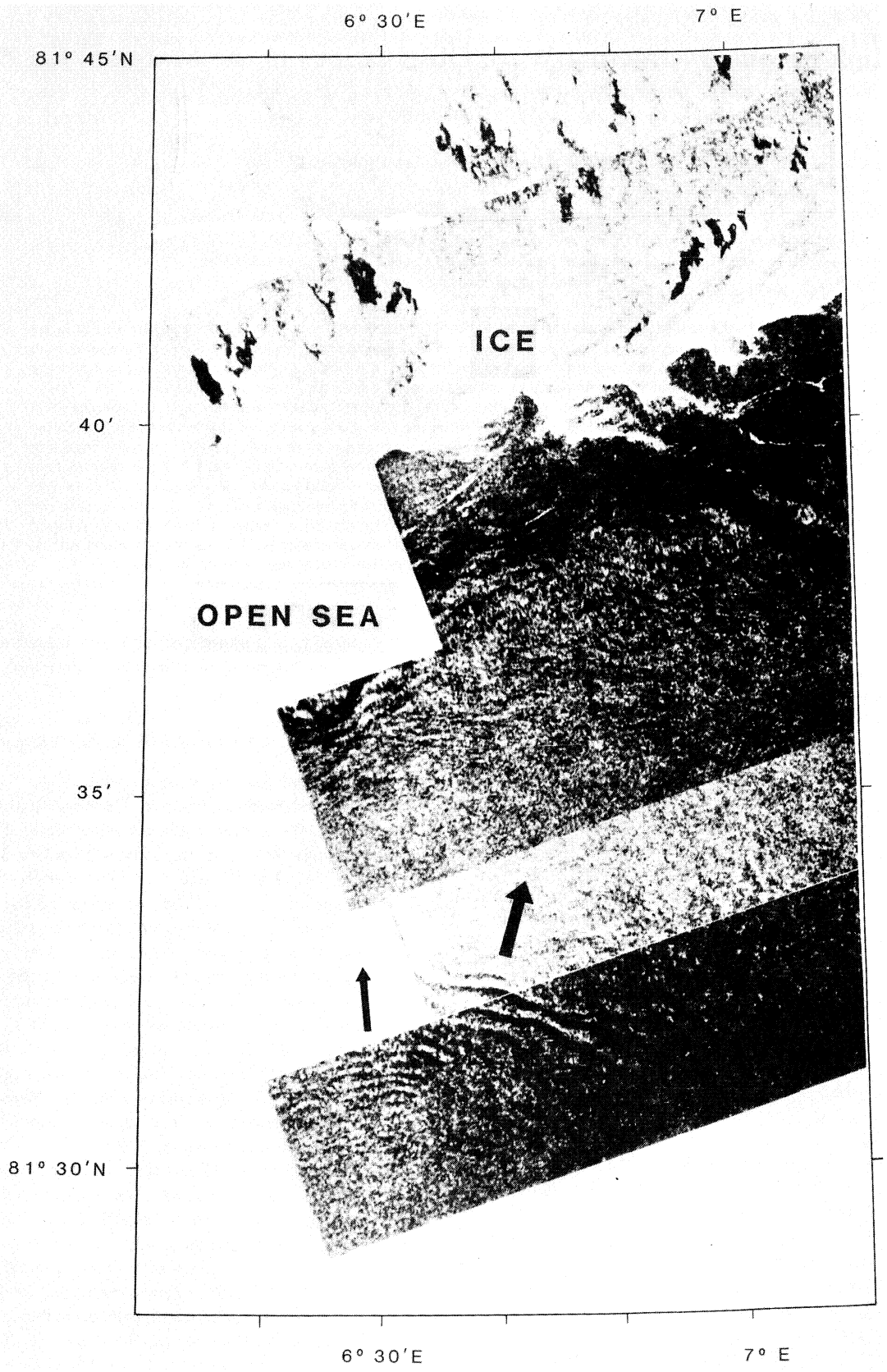

Fig. 1. Synthetic aperture radar (SAR) image from September 19, 1979, during the NORSEX experiment, showing the ice edge and internal waves in the open ocean. The thin and thick arrows indicate the propagation of waves with 400-m and 1000-m wavelength, respectively. [After *Johannessen et al.*, 1983].

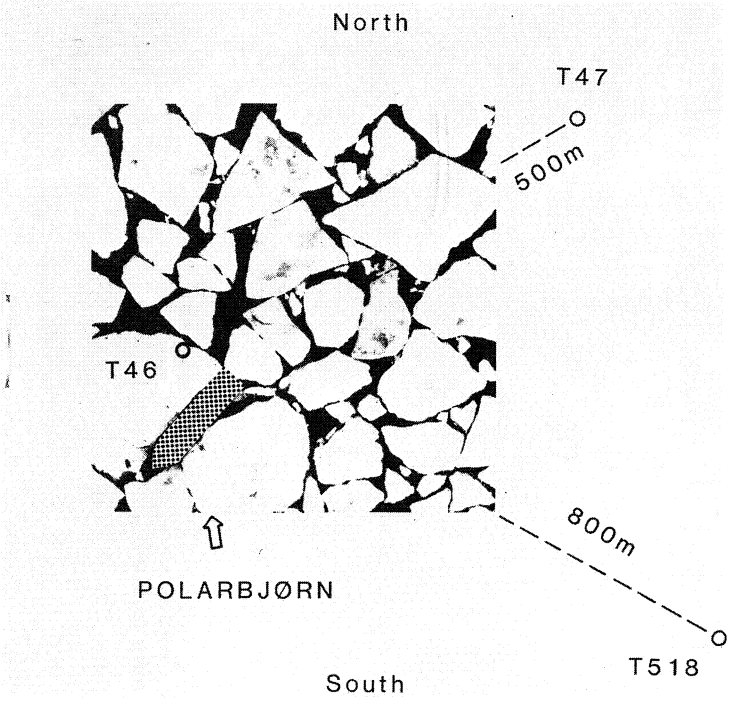

Fig. 2. Thermistor chain locations relative to the *Polarbjørn*. An aerial photograph is superimposed indicating an ice concentration of approximately 90%. The ship is 50 m long.

changed to easterly, causing the ice to turn northwestward. Two days later the wind was again southerly, leading to a northeastward ice drift. The current velocity of the whole water column down to 200 m was northerly, along the isobaths, throughout the period, with a maximum speed of 0.15 m/s at the western slope of the seamount.

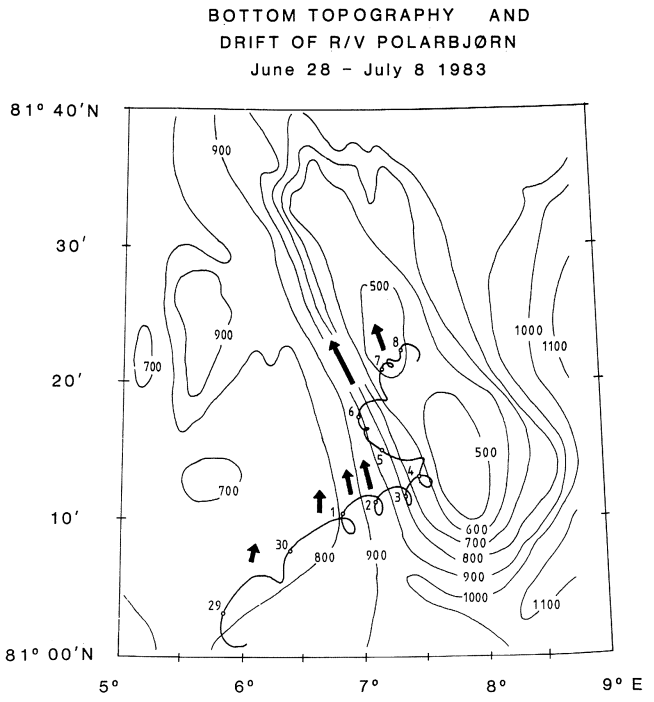

Fig. 3. Chart of the area on the Yermak Plateau north of Svalbard where the internal wave experiment took place. The heavy line is the trajectory of the *Polarbjørn* with date marks. The arrows indicate the mean current at 40 m measured by an Aanderaa current meter. The tidal components are removed, and the highest mean velocity (0.15 m/s) is observed at the slope of the seamount. The depth contours are in meters.

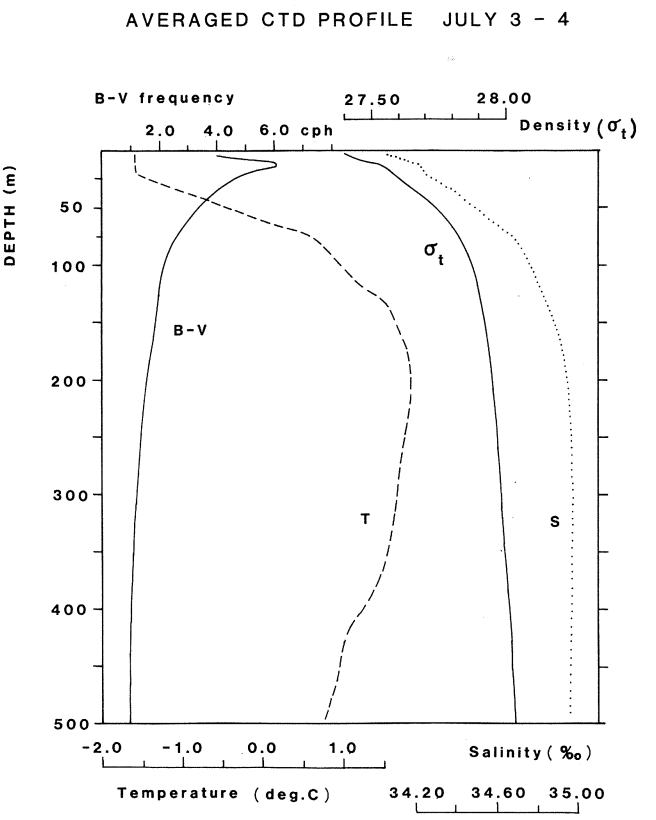

Fig. 4. Profiles to 500 m of temperature, salinity, σ_t and Brunt-Väisälä frequency averaged over 48 CTD casts on July 3–4.

CTD data were obtained approximately every hour down to the bottom, which varied between 500 m and 900 m. They were used to provide the Brunt-Väisälä frequency as a function of depth and time. An average CTD profile for July 3–4 is plotted in Figure 4 for temperature, salinity, σ_t, and Brunt-Väisälä frequency. The upper 20 m has cold water (from $-1.5°$ to $-1.7°$C), and the salinity increases from about 34.00‰ at the surface to about 34.30‰ at 30 m. Below this top layer the CTD data show that the temperature is a good indicator of the density field and can therefore be used for IW studies.

3. Data Description

Contoured plots of isotherm depths as a function of time were produced for all 7 days of thermistor data. During a 24-hour period, starting at 1100 UT on July 3, most of the thermocline was displaced above 65 m, allowing the isotherms between $-1.7°$ and 0.0°C to be continuously displayed (Figure 5). Therefore this period was selected for a case study. The predominant features are the ubiquitous vertical oscillations indicating IW activity over a broad frequency band. The most intense oscillations are interpreted as a wave train and can be seen at all three thermistor chains in the period between 2200 UT on July 3 and 0500 UT on July 4. The observed frequencies are 2–3 cycles per hour (cph), and the amplitude is 2–3 m at 30-m depth and increases to 5–6 m at 65 m. The high vertical coherence and the presence of a predominant frequency band, evident in Figure 5, suggest that the wave train can be described as horizontally propagating plane waves of a

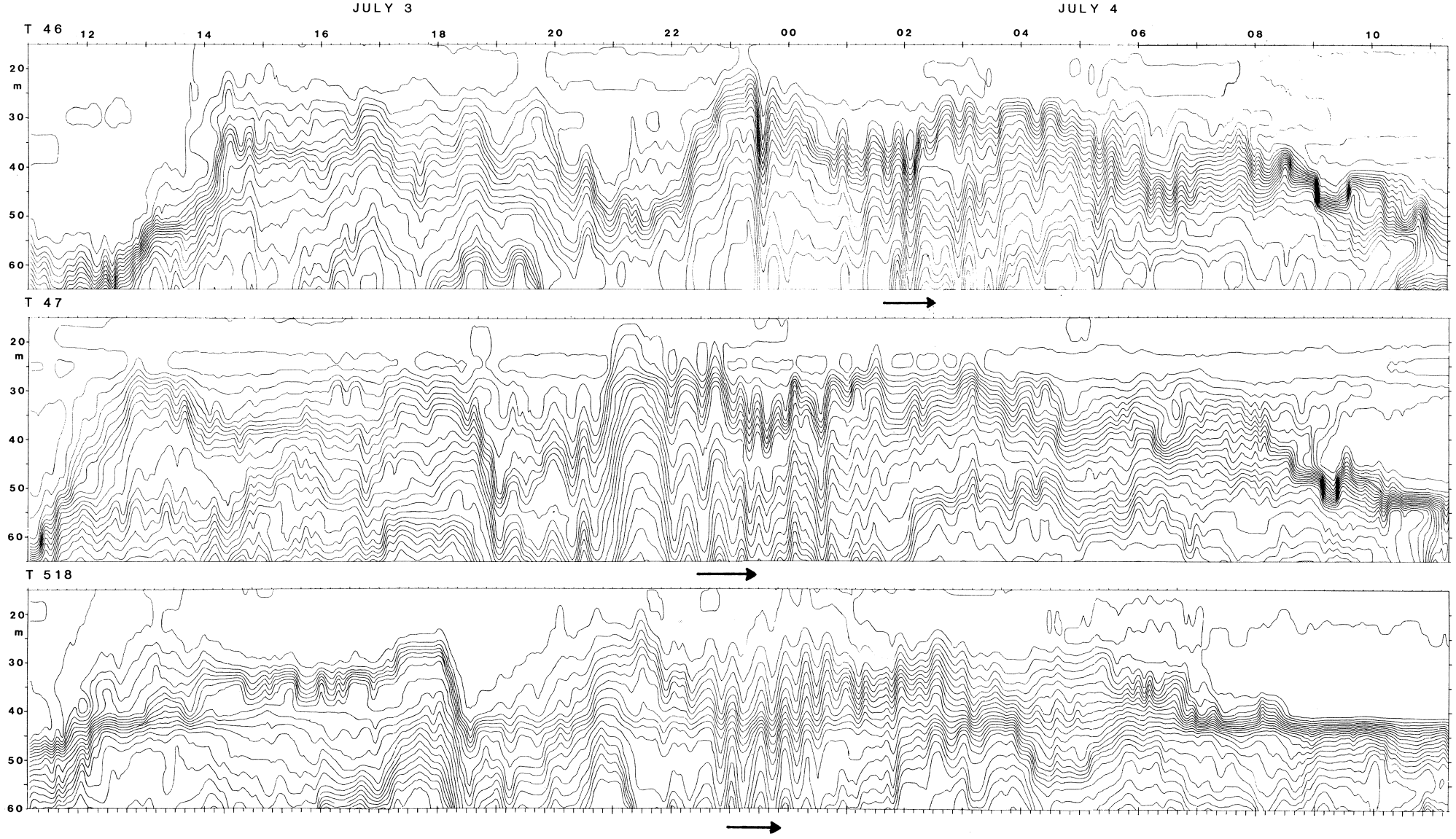

Fig. 5. Contoured plot of temperature as function of time and depth for the three thermistor chains. A period of 24 hours is selected (from July 3, 1100 UT to July 4, 1100 UT) when most of the thermocline was displaced above 65 m. The isotherms are plotted with 0.10°C intervals. The top layer contains cold water of -1.7°C, and the temperature increases with depth. The arrows indicate the passage of the wave train.

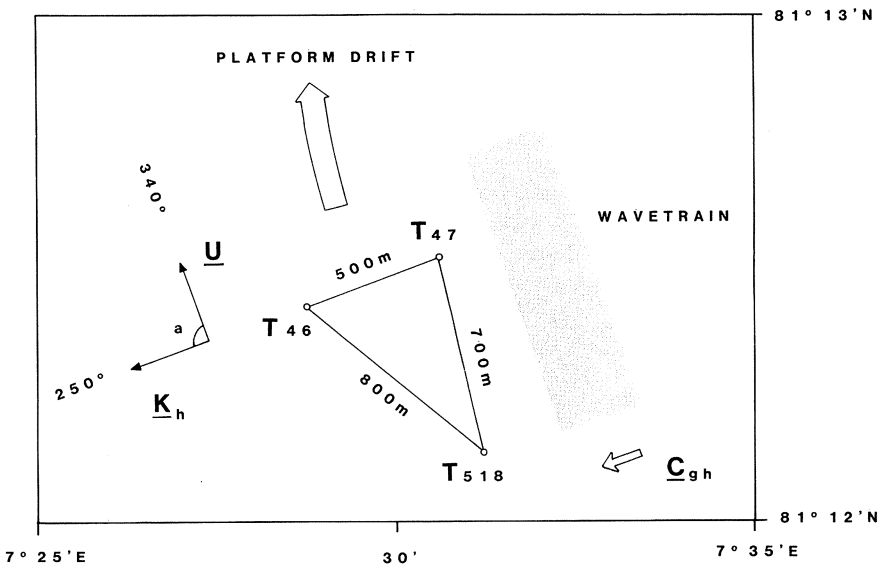

Fig. 6. Size and orientation of the triangle of thermistor chains. The propagation of the wave train, indicated by the shaded area, is in a west-southwestward direction (250°) nearly perpendicular to the platform drift. $\mathbf{C}_{gh}$ is the horizontal component of the group velocity, $\mathbf{K}_h$ is the horizontal component of the wave number vector, and $\mathbf{U}$ is the mean current relative to the platform.

single vertical mode. Based on the assumption of progressive plane waves, it is seen that the wave train arrives first at T47, then at T518 1 hour later, and finally at T46 3 hours later. Knowing the orientation and size of the triangle, these roughly estimated arrival times imply that the wave train propagates west-southwest (250°) with a horizontal group velocity of 0.05 m/s (Figure 6). In this estimate, no correction for the movement of the triangle is necessary because it drifts perpendicular to the wave train. This drift direction excludes the possibility of interpreting the IW observations as a stationary wave train.

From the theory of waves in a continuously stratified fluid [*Turner*, 1973, pp. 21–31] it is known that the horizontal components of the group velocity and the phase velocity are directed in the same sense, while the vertical components are directed in opposite senses. Consequently, the direction of the horizontal component of the wave number $\mathbf{k}$ is also 250°, but its magnitude $|\mathbf{k}|$ is still unknown.

Observations of IW in the presence of a mean current implies that frequencies may be Doppler-shifted, which must be taken into account in the interpretation. Using ice floes as observational platforms would give perfect IW measurements if the ice and the ocean move at the same velocity. However, during the passage of the wave train the observed current, measured relative to the ice floes, is approximately 0.10 m/s and is directed 330°–340° at 20–40 m (Figure 7). The Doppler shift $\mathbf{k} \cdot \mathbf{U}$ modifies the intrinsic frequency ω', such that $\omega = \omega' + \mathbf{k} \cdot \mathbf{U}$, where ω is the observed frequency, $\mathbf{k}$ is the horizontal wave number vector, and $\mathbf{U}$ is the mean current vector relative to the observational platform. If $\mathbf{k}$ and $\mathbf{U}$ are nearly perpendicular to each other, the Doppler shift can be considered minimal. Later in this paper, when $|\mathbf{k}|$ is determined, a quantitative estimate of $\mathbf{k} \cdot \mathbf{U}$ compared to ω will be made and shown to be small.

When the array started to move in a westward direction, on July 4 at 0800 UT (Figure 3), the IW signals became weaker, especially at T518 where the isotherms leveled out. A possible explanation for this sudden decay of the IW is that the triangle starts to move in the same direction and with the same speed as the phase velocity of the wave train. The observed drift speed of the triangle is 0.10–0.15 m/s in this period. The estimated direction of 250° shows that the wave train propagates perpendicular to the isobaths of the seamount from shal-

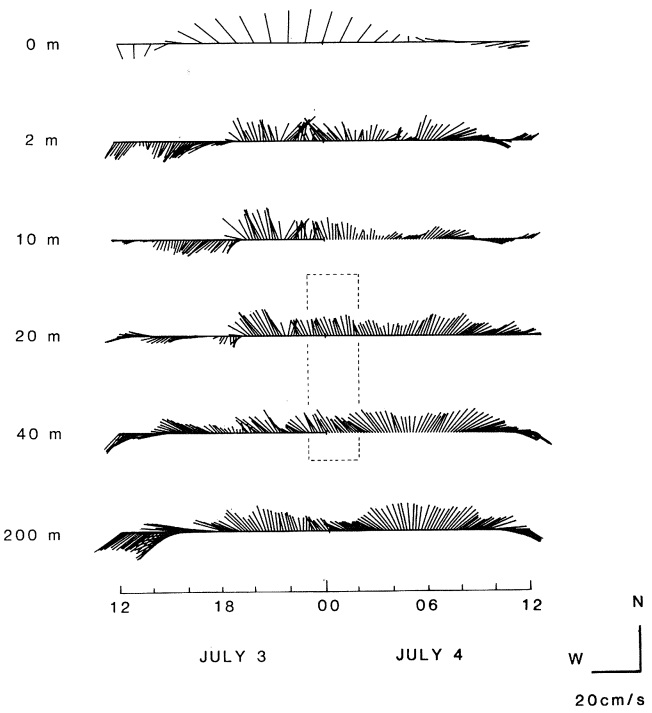

Fig. 7. Hourly values of the velocity vector of the ice drift at 0 m computed from the ship's positions (a low-pass filter with a 6-hour cutoff period has been used to remove high-frequency noise in the navigational data) and unfiltered current vectors at 2 m to 200 m measured relative to the ship at 10-min intervals by Aanderaa current meters. Northerly and westerly current vectors with scale are indicated in the lower right corner. The dashed box indicates the period and depth of the passage of the wave train.

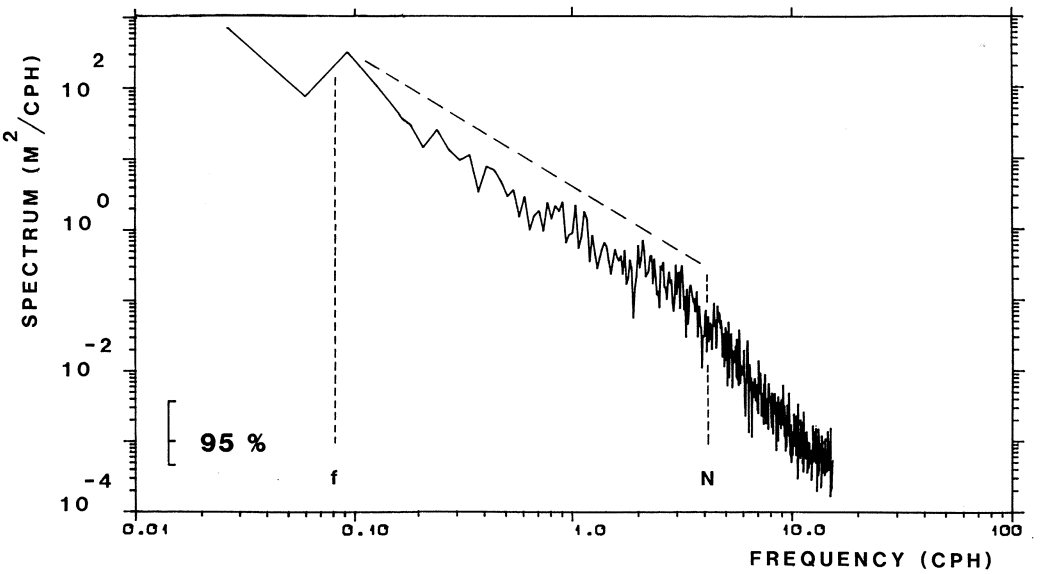

Fig. 8. Vertical displacement spectrum computed from a 7-day temperature series at T47, divided by a mean vertical temperature gradient of 0.10°C/m. The time series is obtained at 60-m depth, where the Brunt-Väisälä frequency is 3–4 cph. The inertial period is close to 12 hours ($f = 0.083$ cph) at 81°N. The spectrum is estimated by fast Fourier transformation (FFT), and the 95% confidence level is based on 10% tapering of the series and smoothing over 5 frequency bands [*Bloomfield*, 1976]. The Garrett-Munk spectrum is plotted using a scaling factor $r = 320$ m² cph and a cutoff frequency $N = 4.0$ cph.

lower to deeper water. It is noteworthy that the IW in Figure 1 also propagate in the same manner, but on the northern side of the seamount. These observations suggest that the bottom topography is of importance in the generation of the wave train.

4. Energy Spectra

Spectral analysis of the whole 7-day period of data was carried out to obtain information about the general IW energy level in this area, but for the case study of the wave train, shorter time series (16 hours) were used in the computation of

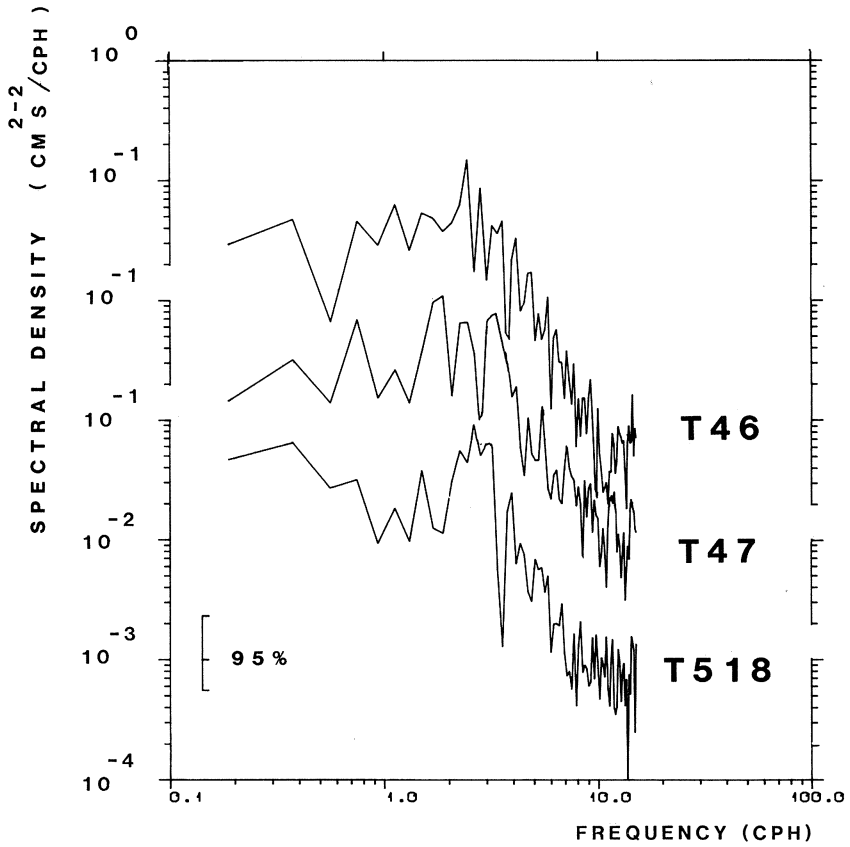

Fig. 9. Vertical velocity spectra for all three thermistor chains computed from time series of the depth of the −0.7°C isotherm. The time series are from July 3, 1600 UT to July 4, 0800 UT. The energy scale is shifted upward by 1 and 2 decades for T47 and T46, respectively. The spectra are smoothed over six frequency bands, yielding a band width of 0.375 cph.

the spectra. Vertical displacement series were computed in two different ways: For method A the depth of given isotherms was computed by vertical interpolation, and for method B the temperature series at fixed sensors were divided by a mean vertical temperature gradient. Energy spectra for the 7-day period were computed based on method B because some of the isotherms were discontinuous in this period, so method A could not be used. In Figure 8 the energy spectrum of T47 at 60 m is shown; this spectrum is based on $dT/dz = 0.10°C/m$ and ranges from less than the inertial frequency f to the Nyquist frequency of 15 cph. Spectral characteristics, such as energy level, a slope of -2 in the IW range between f and N (the local Brunt-Väisälä frequency), and a cutoff at N where the slope increases to approximately -3, are similar at T518 and T46.

The Garrett-Munk spectral model (GM spectrum) for vertical displacement can be formulated as

$$S_z(\omega) = \frac{2}{\pi} r \frac{f}{N} \frac{(\omega^2 + f^2)^{0.5}}{\omega^3} \quad (1)$$

where ω, f, and N are frequencies in cycles per hour and r is a scaling parameter: $r = Eb^2N_0$ where E is a universal, nondimensional energy level, b is the e-folding scale of $N(z)$ and N_0 is the buoyancy frequency scale in cycles per hour [*Munk*, 1981]. This theoretical spectrum is included in Figure 8 for comparison with the observed data. The level of the spectrum is set by using the canonical value $r = 320$ m^2 cph. The spectral level of the observations is lower than the GM spectrum by a factor of 2–3. To adjust the GM spectrum to the observed spectrum, a value of r between 100 and 150 m^2 cph should be used. This value is higher than the values at the FRAM 3 ice camp on the Yermak Plateau in 1981 [*Levine et al.*, 1985], where r had values of 47 and 75 m^2 cph at depths of 67 and 137 m, respectively.

To use spectral analysis on the wave train observed in Figure 5, a 16-hour period between July 3, 1600 UT and July 4, 0800 UT, was chosen for the computation of the vertical displacement series. In this period the depth of each isotherm could be estimated without any ambiguity. Methods A and B both yielded time series with similar spectral characteristics, but the vertical interpolation method (method A) was selected for the analysis because this method avoids fine structure contamination of the spectra. This can be a problem if vertical displacement series are computed by method B [*Neshyba et al.*, 1972]. A total of 15 isotherm depth series, five at each thermistor chain, were computed for spectral analysis. The selected isotherms were $-1.3°$, $-1.1°$, $-0.9°$, $-0.7°$, and $-0.5°$C at mean depths of 36 m, 39 m, 42 m, 46 m, and 51 m, respectively.

The main difference between the 7-day spectrum and the 16-hour spectrum from July 3–4 (not shown) is that the short-period spectrum has a more pronounced peak or shoulder just prior to the cutoff frequency. The shoulder can be explained by the dominance of the wave train at 2–3 cph in the 16-hour period, whereas in the 7-day spectrum this feature is obscured and is not significant in Figure 8. In his extensive spectral analysis of temperature records, *Pinkel* [1975] suggests that the shoulder can be explained by the dominance of the first mode at high frequencies. To give an enhanced picture of the spectral shoulder, vertical velocity time series were computed by time differentiating the vertical displacement series of the $-0.7°$C isotherm at each thermistor chain. Theoretically, the vertical velocity spectrum is equal to the vertical displacement spectrum multiplied by the square of the frequency. Hence the flat part of the spectra below 2 cph in Figure 9 corresponds to the -2 slope of the spectrum in Figure 8, and the peaks between 2 and 3 cph in Figure 9 correspond to the spectral shoulder. The energy peaks near N are explained by *Desaubies* [1975] as due to constructive interference between IW near the turning depth z where $N(z) = \omega'$ (ω' is the intrinsic frequency of the IW). The accumulation of energy in the 2- to 3-cph band is attributed to the trapping of high-frequency IW in the upper 100 m of the ocean where N is greater than 2 cph. The simple modal structure, the nonstationarity, and the anisotropy of such waves have been discussed by several investigators [*Käse and Clarke*, 1978; *Brekhovskikh et al.*, 1975]. Trapped waves can exist if wave packets move into depths of diminishing $N(z)$ and reach the turning depth. This depth acts as a barrier for downward propagation of the waves and causes an upward reflection of the waves. As a wave packet approaches the turning depth, the crests and troughs turn more steeply, and the particle oscillation becomes more vertically directed [*Munk*, 1981]. Several aspects of the present observations support the assumption of trapped wave energy between the turning depth and the surface: (1) direct observation of increased wave amplitude from 30 m down to 60 m, (2) increased spectral energy with depth in the 2- to 4-cph band (not shown here), and (3) peaks in the vertical velocity spectra just below the cutoff frequency (Figure 9). Unfortunately, the data set does not extend beyond 65 m, so a direct verification of the turning depth is not possible. Use of a mean profile of $N(z)$ suggests that the 2- to 3-cph band has turning depths between 100 m and 50 m.

5. Horizontal Coherence and Phase Spectra

Time series of vertical displacement of the selected isotherms were used to compute a number of horizontal coherence and phase spectra between pairs of the thermistor chains. Since the triangle maintained its shape and orientation during the experiment, the horizontal phase differences $\alpha_{i,j}$ (where $i = 1, 2, 3$; $j = 1, 2, 3$; and $i \neq j$) can be used to deduce possible wavelengths and directions of propagation of the wave train. A large number of solutions may exist, but since the direction of propagation is known from the interpretation of Figure 5, the problem is reduced to a search for possible wavelengths L which satisfy

$$L = (360X_{i,j})/\alpha_{i,j} \qquad i = 1, 2 \qquad j = 2, 3 \qquad i \neq j) \quad (2)$$

$$\alpha_{1,2} + \alpha_{2,3} = \alpha_{1,3} \quad (3)$$

where indices 1, 2, and 3 refer to thermistor chain T47, T518, and T46, respectively. $X_{i,j}$ denotes the component of the distance between two thermistor chains along the direction of the wave propagation; $\alpha_{i,j}$ is obtained from the phase spectra for each frequency band but can be shifted $\pm n \times 360°$, which allows n wavelengths to be included in the phase difference between two sensors. The procedure to find L is then to start with $n = 0$ and increase n by 1 until (2) and (3) are satisfied.

Figure 10 shows an example of coherence and phase spectra between the $-1.1°$C isotherms at T46 and T47. Below 0.7 cph the sensors give coherent signals, indicating that motions on time scales larger than 1.5 hours are correlated at a horizontal separation of 500 m. At frequencies higher than 0.7 cph there is no significant coherence except at 2 cph. The resolution of the spectra using 16-hour time series and smoothing over 6 frequency bands is 0.375 cph. At 2 cph the phase difference is approximately 70°, indicating that the signal at T47 leads the

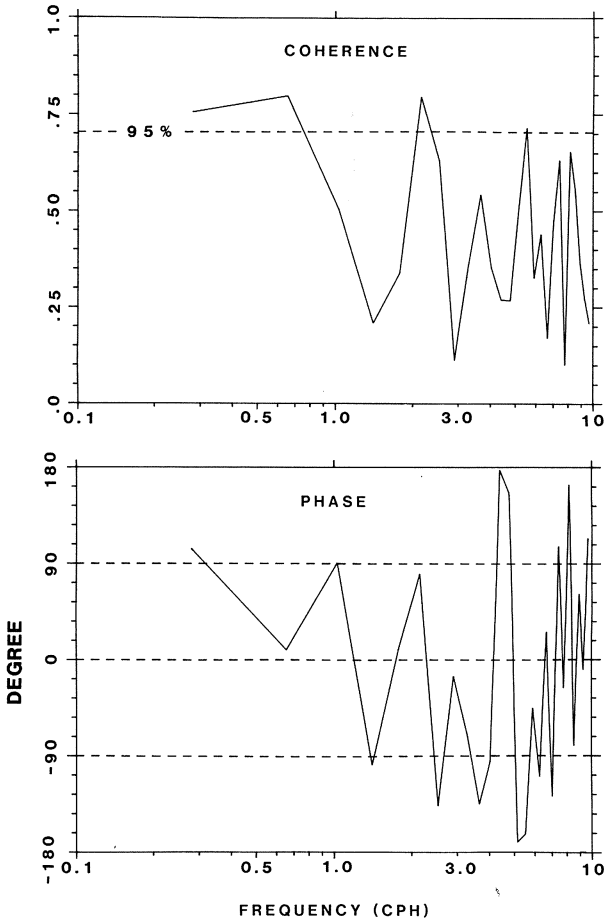

Fig. 10. Horizontal coherence and phase spectra between the −1.1°C isotherms at T46 and T47. By definition, negative phase indicates that T46 leads T47. The bandwidth is 0.375 cph, and the 95% confidence interval for the phase spectrum (not shown) is approximately ±10° at frequencies where the coherence estimate is significant.

signal at T46 by 70°. A 95% confidence interval for the phase estimates (not shown in Figure 10) is less than ±10° for statistically significant coherence estimates [*Bloomfield*, 1976]. A total of 54 coherence and phase spectra were computed showing that the coherence dominated in the bands around 2 and 3 cph. In the computation of a number of phase spectra, some values of $\alpha_{i,j}$ were repeated several times, supporting the assumption that waves with a prevailing direction of propagation are present. Table 1 lists the dominant phase differences, which are coherent at a 95% confidence level.

TABLE 1. Significant Horizontal Coherence Between Pairs of Time Series

Thermistor Pair	Separation, m	Frequency, cph	Phase Difference, deg
T46-T47	500	2.0	+70
		3.0	−80
T518-T46	800	2.0	+120
		3.0	−30
T518-T47	700	2.0	−160
		3.0	−140

Interpretation of the phase differences is as follows: If the phase difference is +80°, series 2 leads series 1 by 80° or series 1 leads series 2 by 80° − 360° = 280°. If the phase difference is −80°, series 1 leads series 2 by 80° or series 2 leads series 1 by 360° − 80° = 280°.

In the 2-cph band a possible interpretation of the phase differences, using Table 1 and allowing an inaccuracy of ±10°, is as follows: $\alpha_{1,2} = 170°$ (T47 leads T518 by 170°, using $n = 0$), $\alpha_{2,3} = 610°$ (T518 leads T46 by 610°, using 110° and $n = 1$), and $\alpha_{1,3} = 780°$ (T47 leads T46 by 780°, using 60° and $n = 2$).

By taking the components of the triangle sides ($X_{1,2}$, $X_{2,3}$, and $X_{1,3}$) along the wave number vector, which is directed 250°, a wavelength $L = 230$ m is estimated. Shorter wavelengths might satisfy (2) and (3) by using larger values for n, but such waves would be of higher modes and are not observed in this study. Furthermore, a phase velocity $c = \omega/k$ corresponding to a wavelength of 230 m is found to be 0.13 m/s. A similar argument for the 3-cph band leads to a wavelength of 135 m and phase velocity of 0.11 m/s. These estimated values of the phase velocity agree with the observations.

6. Computation of the Dispersion Relation

Assuming a linearized equation of motion and the Boussinesq approximation in an incompressible and nonrotating fluid with a mean current yields the vertical velocity equation

$$\frac{d^2W}{dz^2} + Q(z)W = 0 \qquad W(0) = W(-H) = 0 \tag{4}$$

where

$$Q(z) = \frac{N^2(z) - (\omega - \mathbf{k}\cdot\mathbf{U})^2}{(\omega - \mathbf{k}\cdot\mathbf{U})^2}\,\mathbf{k}^2 + \frac{\mathbf{k}\cdot\mathbf{U}''}{(\omega - \mathbf{k}\cdot\mathbf{U})} \tag{5}$$

$W(z)$ is the vertical mode function, H is the bottom depth, $\mathbf{k}$ is the horizontal wave number vector, ω is the frequency, $N(z)$ is the Brunt-Väisälä frequency, and U(z) is the mean current vector.

Equation (4), named after Taylor and Goldstein, takes into account the effect of both stratification and a shear current. *Peters* [1983] has shown that the solution of (4) is strongly influenced by the shear current. Consequently, a quantitative estimate of the terms on the right-hand side of (5) is necessary to see if the shear current is of importance in the present case study. Current measurements, obtained during the passage of the wavetrain, show typical maximum values:

$$U = 0.10 \text{ m s}^{-1}$$

$$\frac{dU}{dz} = 0.3 \times 10^{-2} \text{ s}^{-1}$$

$$\frac{d^2U}{dz^2} = 0.1 \times 10^{-3} \text{ m}^{-1} \text{ s}^{-1}$$

The estimated angle between $\mathbf{k}$ and $\mathbf{U}$ is $a = 90°$ (Figure 6), but a 10° inaccuracy of this value should be allowed. If $a = 80°$, $\mathbf{k}\cdot\mathbf{U}$ is positive and the wave propagation has a downstream component. The observed frequency will then be higher than the intrinsic frequency. Note that the expression $(\omega - \mathbf{k}\cdot\mathbf{U})$ shows the observed frequency modified by the Doppler shift. By inserting observed values for ω, $\mathbf{k}$, and $\mathbf{U}$, this modification is approximately 15% for $a = 80°$. The mean current is therefore strong enough to disturb the 2- to 3-cph frequency band, but a 15% Doppler shift is acceptable because the spectral band width is not better than 0.3 cph. Therefore if the angle a deviates less than 10° from 90°, the Doppler effect can be neglected. Furthermore, to evaluate the effect of the vertical shear, it is necessary to compare the first

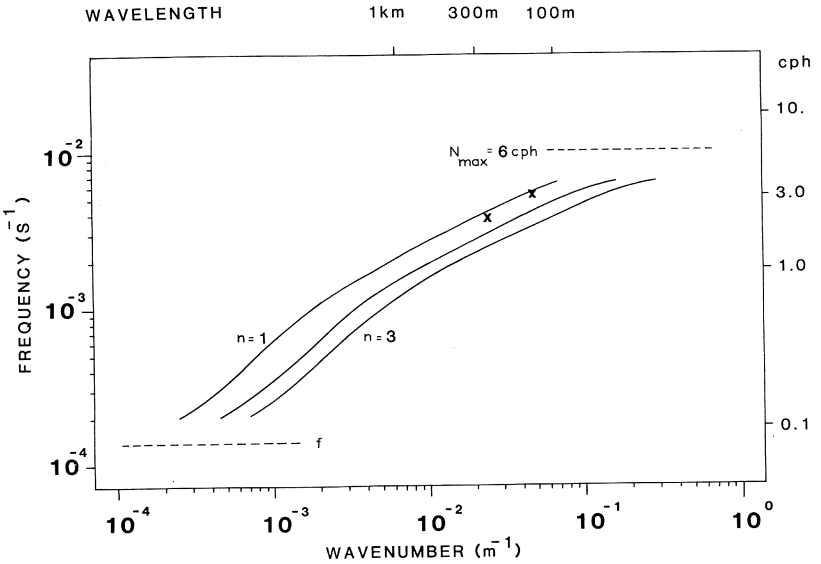

Fig. 11. Dispersion relation for internal waves for the density stratification given in Figure 4, showing the three lowest modes. The crosses indicate wave numbers at 2 cph and 3 cph estimated by phase difference analysis.

and the second term on the right-hand side of (5). Again, by inserting known values of ω, **k**, **U**, **U**″, and $N(z)$, the second term contributes 10–15% to $Q(z)$. Hence the effect of vertical shear can be neglected to first order compared with the effect of stratification. The Taylor-Goldstein equation can then be reduced to the well-known vertical velocity equation for a shearless ocean:

$$\frac{d^2W}{dz^2} + k^2 \frac{N^2(z) - \omega^2}{\omega^2} W = 0 \qquad W(0) = W(-H) = 0 \quad (6)$$

Equation (6) defines the vertical structure of the IW field, using density stratification alone. The solution of this eigenvalue problem yields an infinite, complete, and orthogonal set of modes $W_n(z)$, $n = 1, 2, \cdots$, with eigenvalues k_n, where ω and $N(z)$ are prescribed. The problem is solved numerically using various frequencies ω in the range from 0.2 cph to 6.0 cph. $N(z)$ is computed from the time-averaged and depth-smoothed CTD profile in Figure 4. In this way the dispersion relation for IW, $k = k_n(\omega)$, is established for a given $N(z)$ profile. The depth smoothing was done using a 5-m running mean on the time-averaged density profile. The result is presented in Figure 11, where the first 3 modes are plotted in the range from 0.2 cph to 4.5 cph. In addition, the frequency and wave number relation inferred from the horizontal phase difference analysis is indicated with crosses. The group velocity, $C_g = d\omega/dk$, for the 2- to 3-cph band is 0.05 m/s, which agrees with the observed propagation speed of the wave train. The comparison of observed frequencies and wavelengths with the theoretical dispersion relation shows that the observed wave train on July 3–4 agrees fairly well with first-mode IW.

Since the observations are available only from 30 m to 65 m, limited verification of the vertical mode function can be made. At 3 cph, $W_1(z)$ has a maximum at 15 m and is zero below 50 m, whereas at 2 cph, $W_1(z)$ is maximum at about 70 m and zero below 120 m (not shown). The increasing amplitude of vertical displacement from 30 m down to 65 m agrees with the shape of $W_1(z)$ at 2 cph. However, the fact that the density profile varied during the period when the IW were observed made it necessary to recompute the dispersion relation using slightly different $N(z)$ profiles. In this way the inaccuracy of the dispersion relation attributable to the time variation of the density profiles was estimated. At each frequency the computed wave number varied by at most $\pm 10\%$ compared with the case where the averaged $N(z)$ profile (Figure 4) was used. This is acceptable, since the frequency observations also have a $\pm 10\%$ accuracy.

7. Discussion and Conclusion

Energy spectra of vertical displacement series are compared with the Garrett-Munk spectrum, indicating an energy level that is lower than that model's by a factor of 2–3. However, compared with other observations in the Arctic, the energy level is higher. The questions that arise are, is the MIZ a more active area for IW generation than the interior of the ice-covered ocean, or is it the seamount that causes the wave train? Atmospheric forcing can be discarded as a generating mechanism because the experiment was carried out in a period of calm wind conditions. Tidally generated internal wave packets near topographic features such as straits, banks, seamounts, and fjord sills have been reported by several investigators [*Haury et al.*, 1979; *Apel and Gonzalez*, 1983], but their reports are from shallow areas where the pycnocline is directly disturbed by the topography. In the present case the seamount is much deeper than the pycnocline and can probably cause high-frequency IW only indirectly. It has been shown that the vertical shear can be neglected compared with stratification in the area where the experiment took place. However, outside this area, tidally induced vertical shear large enough to generate high frequency IW may occur temporarily. These waves may then propagate into an area of smaller vertical shear.

The interactions between sea ice and IW have been discussed by *Muench et al.* [1983]. They demonstrated how IW can be generated by the stress discontinuity in the marginal ice zone. Another explanation for the IW is that ridges underneath the ice floes (ice keels) can generate internal waves if the ice floes move in relation to the ocean. This is analogous to lee waves generated in the presence of a mean current flowing over a topographic feature. The distribution of pressure ridge ice keels in the Arctic Ocean has been investigated by *Wad-*

hams [1985], and ice drafts as deep as 40 m were observed in the interior of the pack ice. In the MIZ the mean ice draft varied between 3 and 6 m. Ice keel generation of IW was studied in a laboratory experiment by *Hachmeister and Rigby* [1980], who found that stationary IW could be generated with crests moving perpendicular to the mean flow. The present data show that the ice moves in relation to the water at a typical speed of 0.10 m/s. High-frequency IW with phase velocity equal to the relative current can then be excited as standing waves relative to the ice. When the current changes direction, as it does because of its tidal character, the waves can start to propagate. During MIZEX '87/'89, major IW experiments will be carried out to further investigate the generating mechanisms.

In conclusion, a case study shows that an observed high-frequency internal wave train can be modeled, to a first approximation, as horizontally propagating plane gravity waves of first vertical mode in a shearless ocean, moving in a well-defined direction.

Acknowledgments. The experiment was funded by the Geophysical Institute, Division for Physical Oceanography, University of Bergen, Norway, and Office of Naval Research contract N00014-76-C-0004.

REFERENCES

Apel, J. R., and F. I. Gonzalez, Nonlinear features of internal waves off Baja California as observed from the Seasat imaging radar, *J. Geophys. Res.*, *88*(C7), 4459–4466, 1983.

Bloomfield, P., *Fourier Analysis of Time Series, An Introduction*, John Wiley, New York, 1976.

Brekhovskikh, L. M., K. V. Konjaev, K. D. Sabinin, and A. N. Serikov, Short-period internal waves in the sea, *J. Geophys. Res.*, *80*(6), 856–864, 1975.

Desaubies, Y. J. F., A linear theory of internal wave spectra and coherences near the Vaisala frequency, *J. Geophys. Res.*, *80*(6), 895–899, 1975.

Hachmeister, L. E., and F. A. Rigby, Laboratory studies of stratified flow interaction with topography, in *Proceedings, Second IAHR Symposium on Stratified Flows*, vol. 2, pp. 623–635, Tapir, Trondheim, Norway, 1980.

Haury, L. R., M. G. Briscoe, and M. H. Orr, Tidally generated internal wave packets in Massachusetts Bay, *Nature*, *278*, 312–317, 1979.

Johannessen, O. M., J. A. Johannessen, J. H. Morison, B. A. Farrelly, and E. A. S. Svendsen, The mesoscale oceanographic conditions in the marginal ice zone north of Svalbard in early fall 1979, *J. Geophys. Res.*, *88*(C5), 2755–2769, 1983.

Johannessen, O. M., J. A. Johannessen, S. Sandven, and K. L. Davidson, Preliminary results of the Marginal Ice Zone Experiment (MIZEX) summer operations, in *The Nordic Seas*, edited by B. G. Hurdle, pp. 665–679, Spring, New York, 1985.

Käse, R. H., and R. A. Clarke, High frequency internal waves in the upper thermocline during GATE, *Deep Sea Res.*, *25*, 815–825, 1978.

Levine, M. D., C. A. Paulson, and J. H. Morison, Internal waves in the Arctic Ocean: Comparison with lower-latitude observations, *J. Phys. Oceanogr.*, *15*, 800–809, 1985.

MIZEX Group, MIZEX East 83/84: The summer marginal ice zone program in the Fram Strait/Greenland Sea, *Eos Trans. AGU*, *67*, 513–517, 1986.

Morison, J. H., Internal waves in the Arctic Ocean: A review, *Geophysics of Sea Ice*, edited by N. Untersteiner, pp. 1163–1183, Plenum, New York, 1986.

Muench, R. D., P. H. LeBlond, and L. E. Hachmeister, On some possible interactions between internal waves and sea ice in the marginal ice zone, *J. Geophys. Res.*, *88*, 2819–2826, 1983.

Munk, W. H., Internal waves and small-scale processes, in *Evolution of Physical Oceanography: Scientific Surveys in Honor of Henry Stommel*, edited by B. A. Warren and C. Wunsch, pp. 264–291, MIT Press, Cambridge, Mass., 1981.

Neshyba, S. J., V. T. Neal, and W. W. Denner, Spectra of interval waves: In situ measurements in a multiple-layered structure, *J. Phys. Oceanogr.*, *2*, 91–95, 1972.

Peters, H., The kinematics of a stochastic field of internal waves modified by a mean shear current, *Deep Sea Res.*, *30*, 119–148, 1983.

Pinkel, R., Upper ocean internal wave observations from FLIP, *J. Geophys. Res.*, *80*, 3892–3910, 1975.

Turner, J. S., *Buoyancy Effects in Fluids*, Cambridge University Press, New York, 1973.

Wadhams, P., The ice cover, in *The Nordic Seas*, edited by B. G. Hurdle, pp. 21–86, Springer, New York, 1985.

O. M. Johannessen, Geophysical Institute, University of Bergen, Allegt. 70, Bergen, Norway.

S. Sandven, Nansen Remote Sensing Center, Edvard Griegsvei 3A, 5037 Solheimsvik, Bergen, Norway.

(Received July 15, 1986;
accepted December 29, 1986.)